

## The GBT Pointing Model

Kim Constantikes

**GBT Archive: PR065**

File: Projects

Keys: Pointing

### Abstract

While the angular position of the main beam of the GBT is close-loop controlled using encoders on the mount axes, the actual position of the beam in topocentric coordinates is subject to a variety of perturbing influences, both quasi-random and deterministic. This document is a consolidation of a variety of topics associated with the construction of a static pointing model for the GBT that includes geometrical, gravitational, thermal, track, wind, inertial, and non-ideal material effects. There will be a companion document describing techniques for estimating the model parameters from meteorological, astronomical, and metrological data.

### History

**53.0 KTC 12/6/2006. Original draft.**

**53.1 KTC 6/3/2008. Various additions and corrections.**

## Table of Contents

<b>1</b>	<b>Introduction</b>	<b>4</b>
<b>2</b>	<b>Preliminaries</b>	<b>4</b>
2.1	<i>Cartesian coordinates and transformations</i>	4
2.2	<i>Curvilinear coordinates</i>	5
2.3	<i>Small angle perturbations, similarity, and linearity</i>	5
2.4	<i>Influence coefficients and plate scales</i>	6
2.5	<i>The design coordinate systems</i>	6
<b>3</b>	<b>The pointing model</b>	<b>7</b>
3.1	<i>The ideal pointing model</i>	8
3.2	<i>Geometrical errors in the ideal model</i>	8
3.2.1	Azimuth encoder offset and track tilt	9
3.2.2	Elevation encoder offset and elevation axle skew	10
3.2.3	Optical alignment	10
3.2.4	The pointing model	10
3.3	<i>Gravitational distortions</i>	11
3.3.1	Translation and rotation of optical elements	11
3.3.2	Deflection of the alidade	12
3.3.3	Rotation of the elevation encoder	14
3.3.4	Combined geometric and gravity pointing model	15
3.3.5	Focus tracking and active surface servomechanisms	16
3.4	<i>Track irregularity</i>	16
3.4.1	Local tilt	17
3.4.2	Alidade twist	18
3.4.3	Elevation encoder rotation	20
3.4.4	Combined geometric, gravity, and track pointing model	20
3.5	<i>Thermal effects</i>	21
3.5.1	Differential expansion	22
3.5.2	Modulus of elasticity	22
3.6	<i>Wind effects</i>	22
3.7	<i>Inertial effects</i>	22
3.8	<i>Encoder errors</i>	23
3.8.1	Windup	23
3.8.2	Alignment	23
3.8.3	Cyclic error	24
3.8.4	Nonlinearity	24
<b>4</b>	<b>Additional modeling topics</b>	<b>24</b>
4.1	<i>Refraction correction</i>	24
4.2	<i>Inverting the model</i>	24
4.3	<i>Model parameter stability</i>	24

4.4	<i>Error budgets</i>	25
<b>5</b>	<b>Parameter estimation topics</b>	<b>25</b>
<b>6</b>	<b>Summary and recommendations</b>	<b>25</b>

## Figures

<b>Figure 1.</b>	<b>Local tilt.</b>	<b>18</b>
<b>Figure 2.</b>	<b>Alidade Twist</b>	<b>19</b>
<b>Figure 3.</b>	<b>Alidade free body diagram.</b>	<b>27</b>
<b>Figure 4.</b>	<b>Foci Arrangements and Coordinate Systems for the GBT, Sheet 1.</b>	<b>28</b>
<b>Figure 5.</b>	<b>Foci Arrangements and Coordinate Systems for the GBT, Sheet 2.</b>	<b>29</b>
<b>Figure 6.</b>	<b>Foci Arrangements and Coordinate Systems for the GBT, Sheet 3.</b>	<b>30</b>
<b>Figure 7.</b>	<b>Foci Arrangements and Coordinate Systems for the GBT, Sheet 4.</b>	<b>31</b>
<b>Figure 8.</b>	<b>Foci Arrangements and Coordinate Systems for the GBT, Sheet 5.</b>	<b>32</b>

## Tables

<b>Table 1.</b>	<b>Design coordinate frames in meters and radians.</b>	<b>7</b>
<b>Table 2.</b>	<b>Correspondence of pointing model coefficients for geometrical errors.</b>	<b>11</b>
<b>Table 3.</b>	<b>Geometry and gravity pointing model.</b>	<b>16</b>
<b>Table 4.</b>	<b>Geometry, gravity, and track pointing model.</b>	<b>21</b>

## 1 Introduction

The goal for pointing accuracy and stability of the GBT is, for the highest frequency operation currently envisioned, in the 1"-2" range. Our objective is to provide this kind of pointing performance over as large a fraction of the environmental conditions as possible, e.g., day-night and with wind. Another objective is to reduce the need for observation dedicated to maintaining the pointing model to the barest minimum.

This document develops a pointing model from basic assumptions, and for the Gregorian configuration only since the pointing requirements for the low frequency receivers at prime focus are much less stringent and easily met. The discussion is somewhat pedantic since the notation and methods will be used in other documents. The model is a static model only: Effects such as structural vibration and dynamical servo errors are not considered. We do not consider the effect that aberration may have on pointing, e.g. the bias caused by coma.

There will be a companion document that addresses the estimation of pointing model coefficients from astronomical observations and PTCS instruments, e.g., inclinometers, and assessment of pointing performance in comparison with the requirements<sup>1</sup>.

## 2 Preliminaries

Constructing a model of the GBT pointing requires work in a variety of coordinate systems associated with the alt-az mount, various optical and mechanical elements, and distortions of the structure itself.

### 2.1 Cartesian coordinates and transformations

The first quantities of interest are vectors (free vectors) that have magnitude and direction such as forces. Let  $\vec{r}^i$  be a vector in the  $i^{\text{th}}$  Cartesian coordinate frame. Then

$$\vec{r}^i = R_j^i \vec{r}^j \quad (1)$$

where  $R_j^i$  is a rotation matrix that performs the alias transformation of the vector from the  $j^{\text{th}}$  coordinate basis to the  $i^{\text{th}}$  basis. An alias rotation (also called passive) rotates the coordinates rather than rotating the vector in a coordinate system (called an alibi or active rotation). All rotations in this document are alias unless otherwise noted. The components of  $r$  will be denoted as  $(x_1, x_2, x_3)$  where  $x_1$  corresponds to the usual  $x$ ,  $x_2$  to the usual  $y$ , etc., so that  $\vec{r} = x_1 \hat{x}_1 + x_2 \hat{x}_2 + x_3 \hat{x}_3$  where the circumflex (^) indicates a unit vector. When the coordinate systems are orthogonal, the rotation matrix is a real and orthogonal so

$$\left(R_j^i\right)^{-1} = R_i^j = \left(R_j^i\right)^T \quad (2)$$

where T indicates the transpose. Alibi rotations are just the inverse of the corresponding alias rotation.

Some care must be exercised to distinguish true (or polar) vectors or scalars, such as force, from pseudo-vectors or pseudo scalars, such as angular momentum. Pseudo-vectors will undergo a sign change under an improper rotation, i.e., when the determinate of the real orthogonal rotation matrix is -1. Note the simple mnemonic of the subscript being the "from" coordinate system and the superscript being the "to" coordinate system (for rotation matrices) or the basis (coordinate system) for the vector. Hence a subscript will "cancel" the superscript to its right as in

$$\vec{r}^k = R_j^k R_i^j \vec{r}^i. \quad (3)$$

Position (or bound) vectors transform differently as the translations of coordinate systems must be accounted for. Thus a bound vector will transform as

$$\vec{r}^i = R_j^i \vec{r}^j + o_j^i \quad (4)$$

where  $o_j^i$  is the position vector of the origin of the  $j$  coordinate system in  $i$  coordinates. The distinction between bound and free vectors will be made by the context.

## 2.2 Curvilinear coordinates

There are cases where a more natural or convenient coordinate system is not the usual Cartesian one. For example, the deviations of the primary mirror from an ideal paraboloid of revolution are more conveniently expressed in an  $u$ - $v$ - $w$  coordinate system where the unit vectors  $\hat{u}, \hat{v}, \hat{w}$  form a right-handed orthogonal system with the  $\hat{w}$  vector normal to the parabolic surface at the location  $(u, v)$ , and both  $u$  and  $v$  are positions on level curves such as the hoop and spoke description of the surface. More on this topic is not within the scope of this document, but will become germane in later discussions concerning distortions of optical elements.

## 2.3 Small angle perturbations, similarity, and linearity

Once the basic geometrical components of the pointing model have been formulated we are generally left with very small perturbations to pointing. These small angle rotations have a desirable property that the rotation matrices commute to the 1<sup>st</sup> order (and thus the order of rotations is not important as opposed to say, the Euler angle convention for large rotations), and can be represented as

$$S_i^j = I + \varepsilon_i^j \quad (5)$$

where the matrix  $\varepsilon_i^j$  is skew-symmetric and we will use  $S$  to distinguish this as a small angle rotation. For a positive right hand rule for rotation and alias transformation,

$$\varepsilon = \begin{bmatrix} 0 & \alpha_3 & -\alpha_2 \\ -\alpha_3 & 0 & \alpha_1 \\ \alpha_2 & -\alpha_1 & 0 \end{bmatrix} \quad (6)$$

where  $\alpha_1$  is rotation around the 1-axis (the usual  $x$  axis), etc.

A rotation matrix is a linear operator with an associated basis (coordinate system). The basis of the rotation can be changed via similarity transformation in order to allow us to change the order of the application of a chain of rotations. For example, given the chain

$$\vec{r}^k = R_j^k R_i^j \vec{r}^i. \quad (7)$$

We can change the rotation order by transforming the first rotation. Let

$$\bar{R}_j^k = R_j^i R_j^k R_i^j \quad (8)$$

Then

$$\vec{r}^k = R_i^j \bar{R}_j^k \vec{r}^i = R_i^j R_j^i R_j^k R_i^j \vec{r}^i = R_j^k R_i^j \vec{r}^i. \quad (9)$$

As desired. This will be useful in order to place all small angle rotations in a particular frame, such as the reflector coordinate frame where the rotations are naturally aligned with the elevation and cross-elevation directions (the spherical unit vectors in the ground based frame). For example, the chain

$$\hat{p}^1 = R_2^1 S_3^2 R_4^3 S_5^4 \hat{p}^5 = \bar{S}_3^2 \bar{S}_5^4 R_2^1 R_4^3 \hat{p}^5 = \bar{S}_5^4 \bar{S}_3^2 R_2^1 R_4^3 \hat{p}^5 \quad (10)$$

where

$$\begin{aligned} \bar{S}_3^2 &= R_2^1 S_3^2 R_1^2 \\ \bar{S}_5^4 &= R_2^1 R_4^3 S_5^4 R_3^4 R_1^2 \end{aligned} \quad (11)$$

Expanding the product  $\bar{S}_5^4 \bar{S}_3^2$  demonstrates that small angle errors sum to the 1<sup>st</sup> order

$$\bar{S}_5^4 \bar{S}_3^2 = (I + \bar{\varepsilon}_5^4)(I + \bar{\varepsilon}_3^2) = I + \bar{\varepsilon}_5^4 + \bar{\varepsilon}_3^2 + \text{higher order terms} \quad (12)$$

and thus we can aggregate the perturbations simply. The most important side effect is that we can now treat each small pointing perturbation separately, i.e., without regard to the frame that it occurs in, as long as the perturbation is similarity transformed appropriately at the end, and simply sum the collection of perturbation matrices.

## 2.4 Influence coefficients and plate scales

Under very general conditions (linearity of the structure) there is a linear relationship between torques or forces applied at some node in the structure to the deflections and rotations of some other node (perhaps the same node) in the structure. Using  $\bar{q}$  and  $\bar{Q}$  to denote vectors of generalized deflections and forces respectively,

$$\bar{q} = C\bar{Q} \quad (13)$$

where  $C$  is referred to as the stiffness matrix. Mixed terms may occur, e.g., a rotation at node  $i$  due to force at node  $j$ . A reciprocity theorem requires that the  $C$  matrix is symmetric, i.e., if a force  $Q_i$  at node  $i$  produces a deflection  $q_j$  at node  $j$ , then the same force applied at node  $j$  will produce the same deflection at node  $i$ . Another consequence of structure linearity is that the effects of the generalized forces or deflections superpose, so we can sum individual effects to determine the net effect of several forces or deflections.

We assume a similar relationship between the rigid body generalized deflections of an optical element, e.g., the subreflector, and the pointing perturbation resulting. These are the plate scales<sup>2</sup> of the element, e.g., pointing error on the sky is a linear function of the translation of the subreflector with respect to its design position. To be more precise, the rigid body deflections are the change in pose and position of e.g. minimum-squared-error (MSE) fit of the ideal element shape with respect to the actual shape of the element\*. This assumption is true only for small deflections, where small is determined by the optical properties of the system- As a practical matter deflections that result in pointing changes on the order of a 1000 arc-seconds or less are acceptably small. Small deflections may also have considerable effect on net wavefront errors and beam properties.

## 2.5 The design coordinate systems

GBT Drawing C35102 Rev C details the design coordinate systems and element orientations. See Figure 4 though Figure 8. The following table is a recapitulation of the drawing, converted to SI units and with

---

\* The metric for best fit surface that has the same position for maximum sensitivity as the actual surface may be other than the MSE.

the enumeration of frames that we will subsequently use. Note that the design coordinates are with respect to idealized (and not necessarily measurable with requisite accuracy) rotations.

Enumeration	C35102 Name	Rotation	Translation	Comments
1	Base			$\hat{x}_1 = East$ $\hat{x}_2 = North$ $\hat{x}_3 = LocalUp$  Vertical reference is track
2	Alidade	$R_2^1 = \begin{bmatrix} -1 & 0 & 0 \\ 0 & -1 & 0 \\ 0 & 0 & 1 \end{bmatrix} \begin{bmatrix} C(\pi - \theta) & -S(\pi - \theta) & 0 \\ S(\pi - \theta) & C(\pi - \theta) & 0 \\ 0 & 0 & 1 \end{bmatrix}$	$o_2^1 = \begin{bmatrix} 0.000 \\ 0.000 \\ 0.000 \end{bmatrix}$	$ R_2^1  = 1$ $\theta = azimuth$  LHR + from North
3	Elevation	$R_3^2 = \begin{bmatrix} 1 & 0 & 0 \\ 0 & S(\phi) & C(\phi) \\ 0 & -C(\phi) & S(\phi) \end{bmatrix}$	$o_3^2 = \begin{bmatrix} 0.000 \\ 0.000 \\ 48.260 \end{bmatrix}$	$ R_3^2  = 1$ $\phi = elevation$  RHR + from horizon
4	Reflector	$R_4^3 = \begin{bmatrix} 1 & 0 & 0 \\ 0 & 1 & 0 \\ 0 & 0 & 1 \end{bmatrix}$	$o_4^3 = \begin{bmatrix} 0.000 \\ -62.983 \\ 5.000 \end{bmatrix}$	$ R_4^3  = 1$
5	Prime Focus	$R_5^4 = \begin{bmatrix} 0 & 0 & 1 \\ C(0.794) & -S(0.794) & 0 \\ S(0.794) & C(0.794) & 0 \end{bmatrix}$	$o_5^4 = \begin{bmatrix} 0.000 \\ 0.000 \\ 60.000 \end{bmatrix}$	$ R_5^4  = 1$
6	Subreflector	$R_6^4 = \begin{bmatrix} 0 & 0 & 1 \\ C(0.641) & -S(0.641) & 0 \\ S(0.641) & C(0.641) & 0 \end{bmatrix}$	$o_6^4 = \begin{bmatrix} 0.000 \\ -4.292 \\ 63.802 \end{bmatrix}$	$ R_6^4  = 1$

Table 1. Design coordinate frames in meters and radians.

### 3 The pointing model

We will now compose the pointing model by first constructing the geometric (ideal) relationship between the base coordinates and the principle ray of the optical system and then consider a sequence of small angle effects. The result will be a parametric model with the estimation of parameters addressed later. Note that azimuth and elevation angles are strictly the error-free encoder angles- Which might not be easily converted to astronomical spherical angles due to the assembly of pointing perturbations. In fact,

the purpose of the pointing model is to provide an invertible relationship between the two. There may be cases where various parameters of the pointing model are not linearly independent, which could present problems in the estimation of these parameters. If so, regularization of the model will need to be addressed to achieve, as much as possible, the uniqueness of a model solution.

### 3.1 The ideal pointing model

The optic is aligned so that the principle ray in the reflector coordinate frame is just  $\hat{x}_3^4 = \hat{p}^4$  where  $\hat{p}^4$  denotes the principle ray in the reflector coordinates. Thus the principle ray in the base coordinate frame is

$$\hat{p}^1 = R_2^1 R_3^2 R_4^3 \hat{p}^4 = \begin{bmatrix} C(\phi)S(\theta) \\ C(\phi)C(\theta) \\ S(\phi) \end{bmatrix}, \quad (14)$$

the base coordinate spherical angles of the principle ray are  $(\theta, \phi)$  as expected

$$\begin{aligned} \phi &= \text{ArcSin}(p_3^1) \\ \theta &= \text{ArcTan}\left(\frac{p_1^1}{p_2^1}\right), \end{aligned} \quad (15)$$

and the spherical unit vectors are

$$\begin{aligned} \hat{p}^1 &= \hat{p}^1 & \hat{\rho}^4 &= \hat{x}_3^4 \\ \hat{\theta}^1 &= \left| \frac{d\hat{p}^1}{d\theta} \right|^{-1} \frac{d\hat{p}^1}{d\theta} = \begin{bmatrix} \text{Cos}(\theta) \\ -\text{Sin}(\theta) \\ 0 \end{bmatrix} & \hat{\theta}^4 &= \hat{x}_1^4 \\ \hat{\phi}^1 &= \left| \frac{d\hat{p}^1}{d\phi} \right|^{-1} \frac{d\hat{p}^1}{d\phi} = \begin{bmatrix} -\text{Sin}(\phi)\text{Sin}(\theta) \\ -\text{Sin}(\phi)\text{Cos}(\theta) \\ \text{Cos}(\phi) \end{bmatrix} & \hat{\phi}^4 &= -\hat{x}_2^4 \end{aligned} \quad (16)$$

where  $\hat{\theta}$  and  $\hat{\phi}$  are the cross-elevation and elevation directions respectively.

### 3.2 Geometrical errors in the ideal model

Geometrical errors are just the errors due to differences between the design frames (actually, the positions and pose of e.g., the elevation axle) and the telescope as constructed. For convenience we will formulate the errors in the cross-elevation and elevation directions, i.e., the pointing error will be expressed as

$$\Delta \bar{p}^4 = -\hat{p}^4 + \tilde{p}^4 = \Delta \theta \hat{\theta}^4 - \Delta \phi \hat{\phi}^4 \quad (17)$$

where  $\tilde{p}^4$  is the measured pointing direction and  $\hat{p}^4$  is the predicted (ideal) pointing direction. The effect of optic rotations is degenerate with elevation axle rotations (see below) but kept separate in anticipation of direct measurements of elevation axle pose using inclinometers.

Since processed<sup>†</sup> astronomical observations (“Jack Scans”) measure pointing errors “on the sky”, or  $\Delta\theta^4$  and  $\Delta\phi^4$ , we note that for some small angle perturbation  $S$  the on the sky error will be the elements of the similarity transformed  $\varepsilon$

$$\begin{aligned}\Delta\bar{p}^4 &= (R_3^4 R_2^3 S R_1^2 - R_3^4 R_2^3 R_1^2) \hat{p}^1 = R_3^4 R_2^3 \varepsilon R_1^2 \hat{p}^1 = \begin{bmatrix} \Delta\theta^4 \\ -\Delta\phi^4 \\ 0 \end{bmatrix} \\ &= (R_3^4 R_2^3 \varepsilon R_3^2 R_4^3) R_3^4 R_2^3 R_1^2 \hat{p}^1 = \bar{\varepsilon} \hat{p}^4\end{aligned}\quad (18)$$

For convenience we enumerate several  $\bar{\varepsilon} \hat{p}^4$  given Table 1:

$$\begin{aligned}\bar{\varepsilon}_1 \hat{p}^4 &= (R_3^4 R_2^3 R_1^2 \varepsilon R_2^1 R_3^2 R_4^3) \hat{p}^4 = \begin{bmatrix} \alpha_3 \text{Cos}(\phi) - \text{Sin}(\phi) \{ \alpha_2 \text{Cos}(\theta) + \alpha_1 \text{Sin}(\theta) \} \\ \alpha_1 \text{Cos}(\theta) - \alpha_2 \text{Sin}(\theta) \\ 0 \end{bmatrix} \\ \bar{\varepsilon}_2 \hat{p}^4 &= (R_3^4 R_2^3 \varepsilon R_3^2 R_4^3) \hat{p}^4 = \begin{bmatrix} \alpha_3 \text{Cos}(\phi) - \alpha_2 \text{Sin}(\phi) \\ \alpha_1 \\ 0 \end{bmatrix} \\ \bar{\varepsilon}_3 \hat{p}^4 &= (R_3^4 \varepsilon R_4^3) \hat{p}^4 = \begin{bmatrix} -\alpha_2 \\ \alpha_1 \\ 0 \end{bmatrix} = \bar{\varepsilon}_4 \hat{p}^4\end{aligned}\quad (19)$$

Note that terms that are second order small occur, e.g.,  $\alpha_3 \text{Cos}(\phi) \alpha_2 \text{Cos}(\theta)$ , which are effectively zero and will be removed when the various contributions are summed.

### 3.2.1 Azimuth encoder offset and track tilt

An offset of the azimuth encoder with respect to true north is a rotation around  $\hat{x}_3^1$  direction, and track tilts are rotations around  $\hat{x}_2^1$  and  $\hat{x}_1^1$ , so

$$\Delta\bar{p}^4 = \bar{\varepsilon}_1 \hat{p}^4 = \begin{bmatrix} \alpha_3 C(\phi) - S(\phi) \{ \alpha_2 C(\theta) + \alpha_1 S(\theta) \} \\ \alpha_1 C(\theta) - \alpha_2 S(\theta) \\ 0 \end{bmatrix}.\quad (20)$$

Note that the tilt of the track is with respect to the topocentric coordinate system used by the astronomical pointing calculations, not with respect to local gravity. In fact, measurements of track tilt using inclinometers combined with astronomical inferences results in a measurement of the deflection of local gravity with respect to topocentric coordinates. The result is in agreement with model predictions of local gravity deflection, on the order of arcseconds. This will be discussed more fully elsewhere.

---

<sup>†</sup> It might be easier (and less prone to error) to use un-processed, direct encoder differences. In this case the model would be formulated with  $\Delta\bar{p}^1$  as the pointing error.

### 3.2.2 Elevation encoder offset and elevation axle skew

Similarly, encoder offset is a rotation around  $\hat{x}_1^2$  and the axle skew is rotations around  $\hat{x}_2^2$  and  $\hat{x}_3^2$ , so

$$\Delta\bar{p}^4 = \begin{bmatrix} \alpha_3 \text{Cos}(\phi) - \alpha_2 \text{Sin}(\phi) \\ \alpha_1 \\ 0 \end{bmatrix}. \quad (21)$$

### 3.2.3 Optical alignment

While plate scales and misalignment of the optical elements could be separately calculated for a net pointing error of the optic with respect to the reflector frame, the result is just a set of linear constraints on the combinations of position and pose errors of the elements. There are 15 degrees of freedom<sup>‡</sup>, but only two observables, the cross-elevation and elevation pointing residuals. The net pointing error due to alignment error is just

$$\Delta\bar{p}^4 = \begin{bmatrix} -\alpha_2 \\ \alpha_1 \\ 0 \end{bmatrix}. \quad (22)$$

### 3.2.4 The pointing model

The composite pointing error is

$$\Delta\bar{p}^4 = \begin{bmatrix} \alpha_{3,a} C(\phi) - S(\phi) \{ \alpha_{2,a} C(\theta) + \alpha_{1,a} S(\theta) \} \\ \alpha_{1,a} C(\theta) - \alpha_{2,a} S(\theta) \\ 0 \end{bmatrix} + \begin{bmatrix} \alpha_{3,e} \text{Cos}(\phi) - \alpha_{2,e} \text{Sin}(\phi) \\ \alpha_{1,e} \\ 0 \end{bmatrix} + \begin{bmatrix} -\alpha_{2,o} \\ \alpha_{1,o} \\ 0 \end{bmatrix} \quad (23)$$

Where the subscripts of  $a$ ,  $e$ , and  $o$  denote contributions from the azimuth, elevation, and optic alignment errors. Collecting terms and removing second order small contributions, we get

$$\Delta\bar{p}^4 = \begin{bmatrix} -\alpha_{2,o} - \alpha_{2,e} \text{Sin}(\phi) + \alpha_{3,e} \text{Cos}(\phi) + \alpha_{3,a} C(\phi) - \alpha_{1,a} S(\phi) S(\theta) - \alpha_{2,a} S(\phi) C(\theta) \\ \alpha_{1,e} + \alpha_{1,o} - \alpha_{2,a} S(\theta) + \alpha_{1,a} C(\theta) \\ 0 \end{bmatrix} = \begin{bmatrix} \Delta\theta \\ -\Delta\phi \\ 0 \end{bmatrix} \quad (24)$$

There are seven independent rotations (the  $\hat{x}_3^4$  rotation is around the pointing direction and hence does not cause a pointing error, but may change polarization), but only five independent coefficients of the two-dimensional trigonometric series- Coefficients for track tilt are present in both the elevation and cross-elevation errors. Note that while the basis functions for the series are

---

<sup>‡</sup> The three rotational degrees of freedom of a receiver feed with respect to the phase center might effect efficiency (and perhaps polarization), but pointing should be unchanged.

not orthogonal on  $\theta \in [0, 2\pi)$ ,  $\phi \in [0, \frac{\pi}{2}]$ , they **are** linearly independent. The correspondence of these terms to the other two pointing model representations is:

Physical Meaning	Error Direction	Basis	Coefficient	GBT TPOINT <sup>3</sup> Coefficient	Condon Series Coefficient <sup>4</sup>
Horizontal Collimation	Cross-elevation	1	$-\alpha_{2,o}$	CA	$d_{0,0}$
El Axle Collimation	Cross-elevation	$S(\phi)$	$-\alpha_{2,e}$	NPAE	$b_{0,1}$
Az Zero	Cross-elevation	$C(\phi)$	$\alpha_{3,a} + \alpha_{3,e}$	IA	$d_{0,1}$
East Tilt	Cross-elevation	$S(\phi)C(\theta)$	$-\alpha_{2,a}$	AW	$b_{1,1}$
North Tilt	Cross-elevation	$S(\phi)S(\theta)$	$-\alpha_{1,a}$	AN	$a_{1,1}$
El Zero	Elevation	1	$-\alpha_{1,e} - \alpha_{1,o}$	-IE	$d_{0,0}$
East Tilt	Elevation	$S(\theta)$	$\alpha_{2,a}$	-AW	$c_{1,0}$
North Tilt	Elevation	$C(\theta)$	$-\alpha_{1,a}$	AN	$d_{1,0}$

Table 2. Correspondence of pointing model coefficients for geometrical errors.

### 3.3 Gravitational distortions

The gravity vector, nominally down in the base coordinates, appears to rotate in the tipping structure coordinates as telescope elevation changes. This, and effects of possible imbalance in the tipping structure requiring torques around the elevation axle, cause varying forces and moments in the structure as elevation angle changes. For this portion of the model we consider the optical elements to be rigid and attached to the massless structure with flexible trusses, i.e., the shape of an element does not change, but its position and orientation within the structure might. Distortion of the elements themselves will cause wavefront errors and potentially pointing errors.

The effects are decomposed into contributions from the optics (tipping structure), the change in pose of the elevation axle, and rotation of the elevation encoder.

#### 3.3.1 Translation and rotation of optical elements

The gravity vector in elevation coordinates, including the effect of elevation axle misalignment, is

$$\begin{aligned} \bar{F}_g^3(\phi) &= S_e R_2^3 R_1^2 \bar{F}_g^1 = S_e R_2^3 R_1^2 \begin{bmatrix} 0 \\ 0 \\ -F_g \end{bmatrix} = \begin{bmatrix} F_g \{ \alpha_{3,e} \cos(\phi) + \alpha_{2,e} \sin(\phi) \} \\ F_g \{ \cos(\phi) - \alpha_{1,e} \sin(\phi) \} \\ -F_g \{ \alpha_{1,e} \cos(\phi) + \sin(\phi) \} \end{bmatrix} \\ \Delta \bar{F}_g^3(\phi) &= \bar{F}_g^3(\phi) - \bar{F}_g^3(0) = \begin{bmatrix} F_g \{ \alpha_{3,e} \cos(\phi) + \alpha_{2,e} \sin(\phi) - \alpha_{3,e} \} \\ F_g \{ \cos(\phi) - \alpha_{1,e} \sin(\phi) - 1 \} \\ -F_g \{ \alpha_{1,e} \cos(\phi) + \sin(\phi) - \alpha_{1,e} \} \end{bmatrix} \end{aligned} \quad (25)$$

Thus the deflections and rotations associated with an element  $i$  will be

$$\Delta q_i^3 = C_i \Delta \bar{F}_g^3 = C_i m_i G \Delta \hat{F}_g^3, \Delta q_i^3 = \begin{bmatrix} \Delta \bar{r}_i^3 \\ \Delta \bar{\alpha}_i^3 \end{bmatrix} \quad (26)$$

And the change in pointing will be

$$\begin{bmatrix} \Delta \theta^3 \\ -\Delta \phi^3 \end{bmatrix} = \begin{bmatrix} t_{11,i} & \cdot & \cdot & \cdot & \cdot \\ \cdot & \cdot & \cdot & \cdot & t_{26,i} \end{bmatrix} C_i \Delta \bar{F}_g^3 \quad (27)$$

where the coefficients  $t_{ij}$  are the plate scales associated with the translation and rotation of the element. For the actual values of the small angle rotations seen in practice, the additional terms (e.g.,  $\alpha_{3,e}$ ) in  $\Delta \bar{F}_g^3(\phi)$  are small enough to drop. However, even though the gravity vector is then always in the vertical plane (in the reflector coordinates), this does not mean that there will be no cross-elevation errors- Rather, this depends upon the nature of stiffness associated with the element mounting. Anticipating that we will estimate this effect using astronomical observations, we can combine the  $T$  and  $C$  matrices and various constants. For any one element, after removing the constant term in  $\Delta \bar{F}_g^3$  we have

$$\begin{bmatrix} \Delta \theta_i^3 \\ -\Delta \phi_i^3 \\ 0 \end{bmatrix} = \begin{bmatrix} \beta_{11,i} & \cdot & \cdot \\ \cdot & \cdot & \cdot \\ \cdot & \cdot & \beta_{33,i} \end{bmatrix} \begin{bmatrix} 0 \\ \cos(\phi) \\ -\sin(\phi) \end{bmatrix} = \Delta \bar{p}_i^3 = \Delta \bar{p}_i^4. \quad (28)$$

Collecting all of the optical elements results in

$$\begin{bmatrix} \Delta \theta^4 \\ -\Delta \phi^4 \\ 0 \end{bmatrix} = \left\{ \sum_i \beta_i \right\} \Delta \hat{F}_g^3 = \begin{bmatrix} \beta_{12} \cos(\phi) - \beta_{13} \sin(\phi) \\ \beta_{22} \cos(\phi) - \beta_{23} \sin(\phi) \\ 0 \end{bmatrix}. \quad (29)$$

### 3.3.2 Deflection of the alidade

The moment around the elevation axle bearings can change as a function of elevation angle due to mass imbalance of the tipping structure. Suppose the position of the center of gravity of the tipping structure is  $\bar{r}_{tcg}^3$  and the mass  $m_t$ . Then the moment applied to the alidade is

$$\begin{aligned} \vec{M}_{tcg} &= \vec{r}_{tcg} \times \vec{F}_{tcg} = m_t G \vec{r}_{tcg}^3 \times \hat{F}_{tcg}^3 \cong m_t G \vec{r}_{tcg}^3 \times \begin{bmatrix} 0 \\ \text{Cos}(\phi) \\ -\text{Sin}(\phi) \end{bmatrix} \\ &= m_t G \begin{bmatrix} 0 & r_{3,tcg}^3 & -r_{2,tcg}^3 \\ -r_{3,tcg}^3 & 0 & r_{1,tcg}^3 \\ r_{2,tcg}^3 & -r_{1,tcg}^3 & 0 \end{bmatrix} \begin{bmatrix} 0 \\ \text{Cos}(\phi) \\ -\text{Sin}(\phi) \end{bmatrix} \end{aligned} \quad (30)$$

Where  $\times$  is the usual vector cross product and we have again approximated the gravity vector in the vertical plane. The cross product can be formulated as a linear operation using a skew-symmetric matrix of the moment arm vector. The reaction of the alidade and elevation drive provides for static equilibrium, i.e. (see Figure 3) the forces and moments applied to the tipping structure must be zero

$$\begin{aligned} \vec{M}_{tcg} + \vec{M}_6 + \vec{M}_9 + \vec{M}_{10} &= \vec{0} = \vec{r}_{tcg} \times \vec{F}_{tcg} + \vec{r}_6 \times \vec{F}_6 + \vec{r}_9 \times \vec{F}_9 + \vec{r}_{10} \times \vec{F}_{10} \\ \vec{F}_{tcg} + \vec{F}_6 + \vec{F}_9 + \vec{F}_{10} &= \vec{0} \end{aligned} \quad (31)$$

Where the elevation drive mechanism produces force tangent to the bull gear (always in the  $\hat{x}_2^2$  direction). The force at the bull gear is determined by the moment relationships

$$\vec{F}_6^2 = \begin{bmatrix} 0 \\ F_{2,6}^2 \\ 0 \end{bmatrix} = \begin{bmatrix} 0 \\ \frac{m_t G}{o_{3,3}^2 - r_{3,6}^2} \{ r_{2,tcg}^3 \text{Sin}(\phi) + r_{3,tcg}^3 \text{Cos}(\phi) \} \\ 0 \end{bmatrix} \quad (32)$$

Where the notation  $r_{3,6}^2$  indicates the 3 component ( $\hat{x}_3^2$  or z direction) of the vector  $\vec{r}_6^2$ . The complete set of constraints requires that

$$\begin{aligned} &\left\{ -F_{1,9}^2 = F_{1,10}^2 \right\} \\ &\left\{ \begin{aligned} F_{2,9}^2 &= F_{2,10}^2 \\ F_{2,9}^2 &= -\frac{F_{2,6}^2}{2} \end{aligned} \right\} \\ &\left\{ \begin{aligned} F_{3,10}^2 &= \frac{1}{2} F_{3,tcg}^2 (r_{1,tcg}^3 - r_{1,9}^3) = -F_{3,9}^2 \\ F_{3,10}^2 + F_{3,9}^2 &= F_{3,tcg}^2 \end{aligned} \right\} \end{aligned} \quad (33)$$

Thus the axial forces (parallel to the elevation axle) remain indeterminate and must be determined with an alternative. Without proof we assert that the functional form must be

$$F_{1,9}^2 = a \text{Sin}(\phi) + b \text{Cos}(\phi). \quad (34)$$

Note that the ‘‘y’’ inclinometer data as a function of elevation<sup>5</sup> at least provides some plausibility that the axial compression/tension is a real effect, and that ‘‘potato chip’’ deformations of the primary may result in turn causing astigmatism in the optical system.

The result of the reactions is to deflect the elevation bearing castings and change the pose of the elevation axle. Let  $\Delta\bar{r}_9$  and  $\Delta\bar{r}_{10}$  be the deflections due to  $\Delta\bar{F}_9$  ( $=\bar{F}_9(\phi)-\bar{F}_9(0)$ ) and  $\Delta\bar{F}_{10}$ .

Noting that the alidade towers have different stiffness (see PTCS Project Note 46) but assuming that to the first order the distance between the elevation bearing centers is constant, the resulting rotation of the axle is

$$\varepsilon = \frac{1}{|\bar{r}_9 - \bar{r}_{10}|} \begin{bmatrix} 0 & \Delta r_{2,9}^2 - \Delta r_{2,10}^2 & -(\Delta r_{1,9}^2 - \Delta r_{1,10}^2) \\ -(\Delta r_{2,9}^2 - \Delta r_{2,10}^2) & 0 & 0 \\ \Delta r_{1,9}^2 - \Delta r_{1,10}^2 & 0 & 0 \end{bmatrix}. \quad (35)$$

Let  $C_i^j$  be the stiffness of node  $i$  with respect to a force applied to node  $j$ . Then by superposition, combining various coefficients, and using the functional form of  $\Delta\bar{F}_6, \Delta\bar{F}_9$  and  $\Delta\bar{F}_{10}$

$$\begin{aligned} \Delta\bar{r}_9 &= C_9^6 \Delta\bar{F}_6 + C_9^9 \Delta\bar{F}_9 + C_9^{10} \Delta\bar{F}_{10} = \bar{a}_9 \cos(\phi) + \bar{b}_9 \sin(\phi) \\ \Delta\bar{r}_{10} &= C_{10}^6 \Delta\bar{F}_6 + C_{10}^9 \Delta\bar{F}_9 + C_{10}^{10} \Delta\bar{F}_{10} = \bar{a}_{10} \cos(\phi) + \bar{b}_{10} \sin(\phi) \end{aligned} \quad (36)$$

By combining stiffness matrices and coefficients we arrive at

$$\varepsilon = \begin{bmatrix} 0 & a_3 \cos(\phi) + b_3 \sin(\phi) & -\{a_2 \cos(\phi) + b_2 \sin(\phi)\} \\ -\{a_3 \cos(\phi) + b_3 \sin(\phi)\} & 0 & 0 \\ a_2 \cos(\phi) + b_2 \sin(\phi) & 0 & 0 \end{bmatrix} \quad (37)$$

And finally determine the change in pointing using ( 19)

$$\begin{aligned} \bar{\varepsilon} \hat{p}^4 &= \begin{bmatrix} \cos(\phi)\{a_3 \cos(\phi) + b_3 \sin(\phi)\} - \sin(\phi)\{a_2 \cos(\phi) + b_2 \sin(\phi)\} \\ 0 \\ 0 \end{bmatrix} \\ &= \begin{bmatrix} \beta_1 + \beta_2 \cos(2\phi) + \beta_3 \sin(2\phi) \\ 0 \\ 0 \end{bmatrix}. \end{aligned} \quad (38)$$

### 3.3.3 Rotation of the elevation encoder

Similarly the elevation axle encoder, attached to the manlift side elevation bearing casting, could experience a rotation due to elevation change and tipping structure mass imbalance. The rotation around the  $\hat{x}_1^2$  direction will be a linear function of the forces applied to the alidade, and so we can directly write

$$\varepsilon = \begin{bmatrix} 0 & 0 & 0 \\ 0 & 0 & \beta_1 \cos(\phi) + \beta_2 \sin(\phi) \\ 0 & -\{\beta_1 \cos(\phi) + \beta_2 \sin(\phi)\} & 0 \end{bmatrix} \quad (39)$$

$$\bar{\varepsilon} \hat{p}^4 = \begin{bmatrix} 0 \\ \beta_1 \cos(\phi) + \beta_2 \sin(\phi) \\ 0 \end{bmatrix}$$

### 3.3.4 Combined geometric and gravity pointing model

Combining the pointing changes due to the effect of gravity yields

$$\begin{bmatrix} \Delta\theta^1 \\ \Delta\phi^1 \\ 0 \end{bmatrix} = \begin{bmatrix} \beta_{12,o} \cos(\phi) - \beta_{13,o} \sin(\phi) + \beta_{1,a} + \beta_{2,a} \cos(2\phi) + \beta_{1,a} \sin(2\phi) \\ -(\beta_{1,e} + \beta_{22,o}) \cos(\phi) - (\beta_{2,e} - \beta_{23,o}) \sin(\phi) \\ 0 \end{bmatrix}. \quad (40)$$

Physical Meaning	Error Direction	Basis	Coefficient	Current Model TPOINT Coefficient	Condon Series Coefficient
Horizontal Collimation	Cross-elevation	1	$-\alpha_{2,o} + \beta_{1,a}$	CA	$d_{0,0}$
El Axle Collimation	Cross-elevation	$S(\phi)$	$-\alpha_{2,e} - \beta_{13,o}$	NPAE	$b_{0,1}$
Az Zero	Cross-elevation	$C(\phi)$	$\alpha_{3,a} + \alpha_{3,e} + \beta_{12,o}$	IA	$d_{0,1}$
East Tilt	Cross-elevation	$S(\phi)C(\theta)$	$-\alpha_{2,a}$	AW	$b_{1,1}$
North Tilt	Cross-elevation	$S(\phi)S(\theta)$	$-\alpha_{1,a}$	AN	$a_{1,1}$
Asymmetric Alidade Twist (Imbalance)	Cross-elevation	$S(2\phi)$	$\beta_{3,a}$		$b_{0,2}$
Symmetric Alidade Twist (Imbalance)	Cross-elevation	$C(2\phi)$	$\beta_{2,a}$		$d_{0,2}$
El Zero	Elevation	1	$-\alpha_{1,e} - \alpha_{1,o}$	-IE	$d_{0,0}$
East Tilt	Elevation	$S(\theta)$	$\alpha_{2,a}$	-AW	$c_{1,0}$

North Tilt	Elevation	$C(\theta)$	$-\alpha_{1,a}$	AN	$d_{1,0}$
Asymmetric Gravity	Elevation	$S(\phi)$	$-\beta_{2,e} + \beta_{23,o}$	HZSZ	$b_{0,1}$
Symmetric Gravity	Elevation	$C(\phi)$	$-\beta_{1,e} - \beta_{22,o}$	HZCZ	$d_{0,1}$

Table 3. Geometry and gravity pointing model.

### 3.3.5 Focus tracking and active surface servomechanisms

Both focus tracking and active surface adjustments to compensate for gravitational distortions have the potential to introduce pointing errors. The servo mechanisms that implement the subreflector motions and primary surface adjustments may fail to achieve the commanded positions due to encoder or position sensor errors and servo control loop error, i.e., failing to drive the difference between commanded and sensed position to zero. For example, the active surface LVDT position sensors are known to have significant non-linearity, and the servo control is a “bang-bang” loop<sup>6</sup>. The linearity of the Stewart Platform link length sensors also anecdotally are nonlinear, and there exists a possibility that the kinematic model of link length to subreflector position and pose is in error due to calibration of the link endpoints. There is also a possibility that the position commands, e.g., intended to adjust focus without causing pointing variations, are incorrectly constructed.

The natures of the error functional forms are largely unknown. Hysteretic errors would cause non-linear and memoried errors (e.g., dependent upon the previous motion’s direction). Kinematic errors would be smooth but with somewhat complicated error dependence upon current position (in the case of the Stewart Platform). Command algorithm errors could be either smooth or discontinuous.

Given current pointing performance it is possible to bound the magnitude of the resulting pointing errors, which are modestly small, and comparison of pointing errors from scans that run in different directions or start from different positions bound the hysteretic effects to similarly small pointing errors. Nonetheless, these potential errors should be remembered when examining the residual pointing error after application of a pointing model. It is likely that they will be one of the dominant limits to pointing accuracy.

### 3.4 Track irregularity

The azimuth track tilt terms included in Table 2 are the global tilts of the best fit plane (BFP) to the entire circumference of the track. Track elevation, however, potentially varies over the circumference due to fabrication, foundation subsidence, wear effects, and thermal effects. These local variations influence pointing by causing a local tilt of the BFP (the BFP with respect to the actual contact points) and by introducing forces and moments at the alidade corner weldments- The interface is overconstrained with 16 contact points (the truck wheels). The suspension of each truck, via spherical truck bearings and flex plates, removes to a great extent two of the three orthogonal forces applied by the track to each corner weldment and two of the three moments (torques). Hence there are a total of eight degrees of freedom for the corners representing one force (nominally in the vertical direction) and one torque (nominally around the radial from the pintle bearing) for each corner, and two additional torques and three forces associated with the reaction of the pintle bearing although the forces in the horizontal plane are nominally zero (See Figure 3). We assume that all wheels are in contact with the track at all times.

The deviation of the track centerline from a plane introduces a pointing shift due to a local tilt (the local best fit plane) and due to distortions of the alidade caused by the forces and moments introduced at the

corner weldments and potentially the pintle bearing. In the absence of detailed information on the various stiffnesses and the actual track profile there is not much to be gained in constructing a detailed description of the kinematics other than to note that there are two symmetries that can be used: Pure tilt must have the form

$$\begin{aligned} \varepsilon_t(\theta) &= \begin{bmatrix} 0 & 0 & -\lambda_{2,t}(\theta) \\ 0 & 0 & \lambda_{1,t}(\theta) \\ \lambda_{2,t}(\theta) & -\lambda_{1,t}(\theta) & 0 \end{bmatrix} = -\varepsilon_t(\theta + \pi) \\ \varepsilon_t\left(\theta + \frac{\pi}{2}\right) &= \begin{bmatrix} 0 & 0 & -\lambda_{1,t}(\theta) \\ 0 & 0 & \lambda_{2,t}(\theta) \\ \lambda_{1,t}(\theta) & -\lambda_{2,t}(\theta) & 0 \end{bmatrix} \end{aligned} \quad (41)$$

and deformation must have a 180 degree asymmetry

$$\varepsilon_d(\theta) = -\varepsilon_d(\theta + \pi) \quad (42)$$

as long as the scale length of track elevation error is large compared to the possible deviation of truck positions from the design locations.

The orthogonal inclinometer sets mounted on the elevation bearings (see PTCS PN 44) are used to measure the rotations of the bearings as a function of azimuth angle, and then detrended for temperature variations, wind effects, the global tilt of the track, and residual structural vibrations. Note that a side effect of the detrending process is an explicit measurement of the AN and AW tilt terms

( $-\alpha_{1,a}$  and  $-\alpha_{2,a}$ ).

### 3.4.1 Local tilt<sup>§</sup>

Serendipitously, the inclinometers indicate that the alidade undergoes a tilt, rather than a deformation, around the  $\hat{x}_2^2$  direction (normal to the plane including the elevation axle and pintle). Let  $\Delta_{\xi_{1,9}}^{\xi^2}(\theta)$ ,  $\Delta_{\xi_{2,9}}^{\xi^2}(\theta)$ ,  $\Delta_{\xi_{1,10}}^{\xi^2}(\theta)$  and  $\Delta_{\xi_{2,10}}^{\xi^2}(\theta)$  be the detrended inclinometer measurements from GBT Project TPTCSKTC041129 for rotation around the  $\hat{x}_1^2$  and  $\hat{x}_2^2$  directions at locations  $\bar{r}_9$  and  $\bar{r}_{10}$  (see Figure 3).  $\Delta_{\xi_{2,9}}^{\xi^2}$  and  $\Delta_{\xi_{2,10}}^{\xi^2}$  agree to a remarkable extent. They approximately exhibit the appropriate 180° asymmetry, as shown in Figure 1. The source of the differences in the asymmetry is not known.

---

<sup>§</sup> The measurements in this section have been substantially improved, with much greater resolution on the track and various corrections. See reference 14.

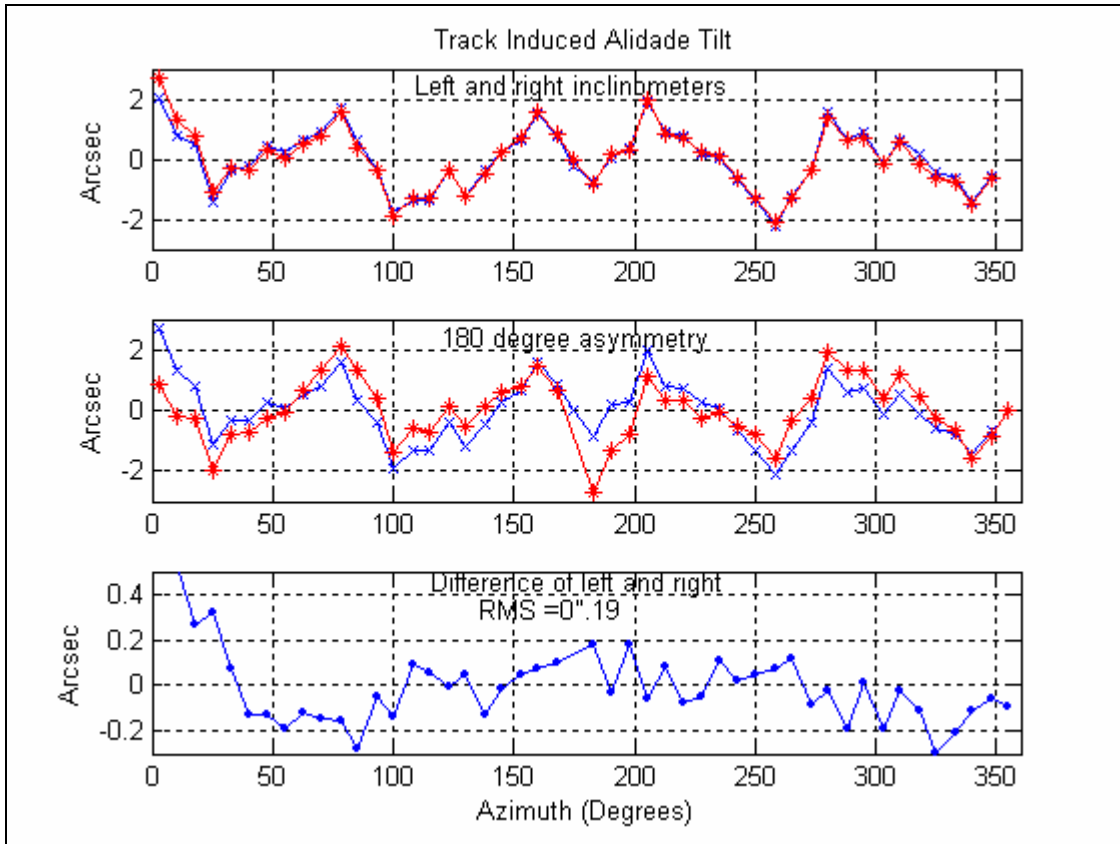


Figure 1. Local tilt.

Since the local tilt has a 90 degree symmetry, we have  $\lambda_{2,t}(\theta) = -\frac{1}{2}[\Delta\xi_{2,9}^2(\theta) + \Delta\xi_{2,10}^2(\theta)]$  and

$\lambda_{1,t}(\theta) = \lambda_{2,t}\left(\theta + \frac{\pi}{2}\right)$  where the signs have been adjusted for the polarities of the inclinometer measurements and the expected value (average) of the two inclinometer angles.

Alidade tilt rather than distortion in this direction is probably due to a much higher stiffness, in turn probably due to the elevation axle itself.

### 3.4.2 Alidade twist

Measurement of the elevation bearing casting rotations in the orthogonal direction, around the  $\hat{x}_1^2$  axis, show that the castings rotate in opposite directions under the influence of track irregularities (Figure 2).

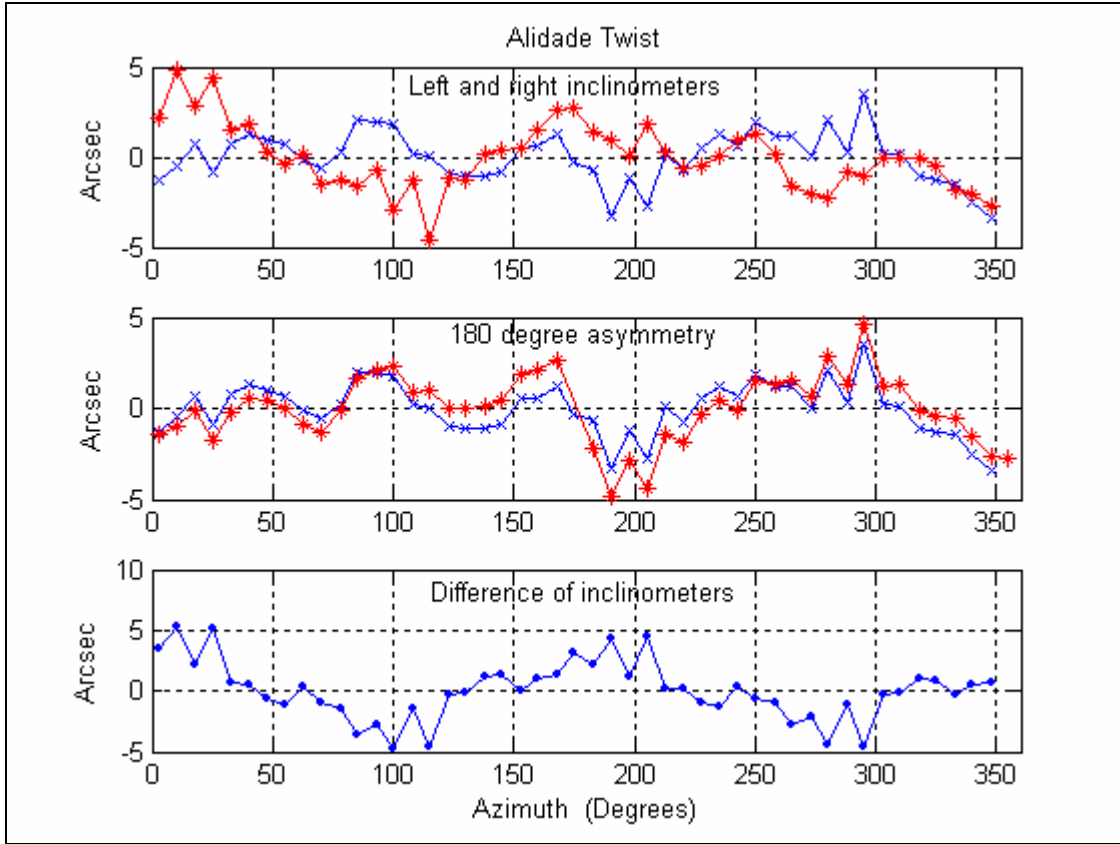


Figure 2. Alidade Twist

Part of the rotation is due to deformation, but part is also due to the local tilt of the alidade. Thus

$$\Delta \xi_{1,9}^2(\theta) = \Delta \tilde{\xi}_{1,9}^2(\theta) + \lambda_{1,t}(\theta) \quad (43)$$

$$\Delta \xi_{1,10}^2(\theta) = \Delta \tilde{\xi}_{1,10}^2(\theta) + \lambda_{1,t}(\theta)$$

Where  $\Delta \tilde{\xi}_{1,9}^2(\theta)$  and  $\Delta \tilde{\xi}_{1,10}^2(\theta)$  are the rotations due to distortion of the alidade. The deflections  $\Delta \bar{r}_9^2$  and  $\Delta \bar{r}_{10}^2$  are linear functions of the respective rotations. The magnitude of the resulting rotation is on the order of arcseconds, so we can approximate the stiffness of the alidade towers as equal without significant error. Thus for  $\Delta \xi_1^2(\theta) = \Delta \xi_{1,9}^2(\theta) - \Delta \xi_{1,10}^2(\theta)$  we have

$$\varepsilon_d(\theta) = \begin{bmatrix} 0 & \lambda_{3,d} & -\lambda_{2,d} \\ -\lambda_{3,d} & 0 & \lambda_{1,d} \\ \lambda_{2,d} & -\lambda_{1,d} & 0 \end{bmatrix} \Delta \xi_1^2(\theta). \quad (44)$$

For this specific case the difference of inclinometers can be approximated as

$$\Delta \xi_1^2(\theta) = 1.6 \sin(2.0\theta - 1.5) + \delta(\theta) \quad (45)$$

where the standard deviation of  $\delta(\theta)$  is  $0''.7$ . This suggests that the twist of the alidade is dominated by large scale error in track elevation rather than moments introduced at the corner

weldments, and could possibly be associated with the circumferential variation of foundation stiffness, e.g. the four grade beam contributions.

### 3.4.3 Elevation encoder rotation

The pointing error due to elevation encoder rotation in the alidade frame will be

$$\varepsilon_e(\theta) = - \begin{bmatrix} 0 & 0 & 0 \\ 0 & 0 & 1 \\ 0 & -1 & 0 \end{bmatrix} \Delta \tilde{\xi}_{1,9}^2(\theta). \quad (46)$$

Note that the mass imbalance rotation (a function of elevation angle, in 3.3.3) is independent of the track induced rotation (a function of azimuth angle).

### 3.4.4 Combined geometric, gravity, and track pointing model

The complete contribution of track irregularity is just the sum of the local tilt, alidade distortion, and elevation encoder rotation errors. The alidade distortion coefficients must be estimated by making measurements with inclinometers concurrently with astronomical pointing runs.

$$\begin{aligned} \lambda_1 &= \lambda_{1,t} + \lambda_{1,d} \Delta \xi_1^2(\theta) + \lambda_{1,e} = \lambda_{1,t} + \lambda_{1,d} \Delta \xi_1^2(\theta) + \lambda_{1,e} (\Delta \xi_{1,9}^2(\theta) - \lambda_{1,t}) \\ &= \lambda_{1,d} \Delta \xi_1^2(\theta) + \Delta \xi_{1,9}^2(\theta) \\ \lambda_2 &= \lambda_{2,t} + \lambda_{2,d} \Delta \xi_1^2(\theta) \\ \lambda_3 &= \lambda_{3,d} \Delta \xi_1^2(\theta) \end{aligned} \quad (47)$$

$$\Delta \bar{p}^4 = \begin{bmatrix} \lambda_3(\theta) \cos(\phi) - \lambda_2(\theta) \sin(\phi) \\ \lambda_1(\theta) \\ 0 \end{bmatrix} \quad (48)$$

Table 4 lists the contributors for the combined geometry, gravity, and track model. Alpha coefficients correspond to geometry terms, beta coefficients correspond to gravity terms, and lambda coefficients correspond to track terms.

Physical Meaning	Error Direction	Basis	Coefficient	GBT TPOINT Coefficient	Condon Series Coefficient
Horizontal Collimation	Cross-elevation	1	$-\alpha_{2,o} + \beta_{1,a}$	CA	$d_{0,0}$
El Axle Collimation	Cross-elevation	$S(\phi)$	$-\alpha_{2,e} - \beta_{13,o} - \lambda_2(\theta)$	NPAE	$b_{0,1}$
Az Zero	Cross-elevation	$C(\phi)$	$\alpha_{3,a} + \alpha_{3,e} + \beta_{12,o} + \lambda_3(\theta)$	IA	$d_{0,1}$
East Tilt	Cross-elevation	$S(\phi)C(\theta)$	$-\alpha_{2,a}$	AW	$b_{1,1}$
North Tilt	Cross-elevation	$S(\phi)S(\theta)$	$-\alpha_{1,a}$	AN	$a_{1,1}$
Asymmetric Alidade Twist (Imbalance)	Cross-elevation	$S(2\phi)$	$\beta_{3,a}$		$b_{0,2}$
Symmetric Alidade Twist (Imbalance)	Cross-elevation	$C(2\phi)$	$\beta_{2,a}$		$d_{0,2}$
El Zero	Elevation	1	$-\alpha_{1,e} - \alpha_{1,o} - \lambda_1(\theta)$	-IE	$d_{0,0}$
East Tilt	Elevation	$S(\theta)$	$\alpha_{2,a}$	-AW	$c_{1,0}$
North Tilt	Elevation	$C(\theta)$	$-\alpha_{1,a}$	AN	$d_{1,0}$
Asymmetric Gravity	Elevation	$S(\phi)$	$-\beta_{2,e} + \beta_{23,o}$	HZSZ	$b_{0,1}$
Symmetric Gravity	Elevation	$C(\phi)$	$-\beta_{1,e} - \beta_{22,o}$	HZCZ	$d_{0,1}$

Table 4. Geometry, gravity, and track pointing model.

### 3.5 Thermal effects

The temperature and temperature gradients of the structure can effect pointing. Gradients cause differential expansions that in turn cause additional stresses in the structure, and there is a small change in the elastic modulus of structural materials as a function of temperature.

The latter effect is almost always ignored as it is very small over normal environmental temperature changes, but when the desired pointing accuracy is very small compared to the pointing-equivalent motion of a component (as it is for the GBT feedarm), relatively small changes in elastic modulus can be significant. The current pointing model has a maximum elevation pointing correction change due to

gravity of about 350" (from zenith to horizon) which is consistent with the expected displacements and the plate scale of feed arm motion. The modulus of carbon steel exhibits a -0.5% / C temperature dependence<sup>7</sup>.

### 3.5.1 Differential expansion

The model and rationale for correction of gradient effects is described in a previous PTCS Project Note<sup>8</sup>. This model could be improved by more temperature sensors and or better algorithms, but the performance to date is adequate for periods where GBT temperatures are not changing rapidly. Particular improvement was obtained in stabilizing focus, somewhat less improvement in elevation pointing, and little improvement in cross-elevation.

### 3.5.2 Modulus of elasticity

The temperature dependence of the modulus is probably only significant in the  $\beta_{22,o}$  and  $\beta_{23,o}$  terms in Table 3 and Table 4. The magnitude of the effect can be approximated by noting that a 1° C bulk feed arm temperature change could cause 1".75 pointing error from zenith to horizon. This effect is not modeled in PFM 5C.

### 3.6 Wind effects

Some attempts have been made to approximate the quasi-static effect of wind on pointing. Hypothesize that the change in pointing is proportional to the kinetic head  $\frac{1}{2} \rho v^2$  with a different constant of proportionality in elevation and cross-elevation, and that the constants are independent of elevation. Then decompose the incident wind velocity into azimuth relative orthogonal components so that

$$\begin{bmatrix} \Delta\theta \\ \Delta\phi \end{bmatrix} = \begin{bmatrix} k_{x-el} & 0 \\ 0 & k_{el} \end{bmatrix} \begin{bmatrix} \{v \sin(\theta - \theta_w)\}^2 \\ \{v \cos(\theta - \theta_w)\}^2 \end{bmatrix}. \quad (49)$$

The off-diagonal terms could be made non-zero (reflecting a belief that the structure reacts in an asymmetric way). The most obvious defect in this model is that it does not take into account the effect of tipping structure pose. Pose effects could be predicted by CFD (computational fluid dynamics) but the structure is complicated enough that it would be infeasible in practice. Alternatively the effect could be estimated using a large dataset including a range of wind speeds for a set of elevation angles, but the existing data are not dense enough in this part of the parameter space for this to yield useful results. Given that the number of parameters to estimate is already quite large (and fitting is ill-conditioned, see below), this model is not included in the current pointing model (PFM 5C).

Dynamical effects are even more problematic: Von-Karman buffeting and pumping of the structure's vibrational modes are conceivably significant, but very hard to model. These effects are also not included in PFM 5C. Instead, model fits utilize data collected with wind speed below some threshold to limit the confounding effects.

### 3.7 Inertial effects

When the structure is moving at constant angular rates centrifugal and Coriolis forces are present. The effects can be bounded by comparison with the gravitational acceleration. Assuming a maximum tracking rate of 250 micro-rad/sec and a maximum 100 m moment arm, the centrifugal forces will be less than  $0.64 \times 10^{-6}$  G, or equivalently a rotation of the apparent gravitational vector of about 0.64 micro-rad. Given that the most sensitive component will be the feed arm and that the pointing effect of an elevation change of 90° is about 350" in gravitational deflection, the effect of centrifugal accelerations will be on the order

of  $0.2'' \times 10^{-3}$ . Coriolis forces will be of the same order given feed arm velocity (in the rotating frame, and due to vibration) of less than 5 mm/sec. Thus neither will be of any consequence.

Tangential acceleration due to dithering of azimuth and elevation input torques is significant but is mediated through the response of the structure as a system of coupled simple harmonic oscillators. This is the subject of current work on modeling and predicting structure vibrational responses and is not appropriately included in a static pointing model. Half-power track experiments<sup>9</sup> show that vibrational pointing errors can be on the order of  $5''$ . We assume that these contributions are incoherent from Jack Scan to Jack Scan, and thus are suppressed when pointing data are fit by the pointing model.

### 3.8 Encoder errors

The BEI electro-optical azimuth and elevation encoders exhibit four types of errors: Less than perfect alignment of the encoder shaft to the telescope axis results in a periodic error, cyclic (fine cycle) encoder errors due to vernier effects, nonlinearities associated with the encoder wheel, and backshaft windup due to encoder friction. A calibration report for one of the installed encoders indicates that the net RMS error (less alignment and windup) is  $0''.63$ .

#### 3.8.1 Windup

Friction in the encoder assembly results in torque applied to the axis backshaft, in turn causing a windup in the backshaft and a resulting hysteretic angle measurement error. Design studies<sup>10</sup> predict an elevation error of  $0''.41$  and an azimuth error of  $0''.69$  for azimuth. If the effect is modeled as a velocity-independent (i.e., non-viscous) term, an indicator of axis rate can be used as a regressor

$$\begin{bmatrix} \Delta\theta \\ \Delta\phi \end{bmatrix} = \begin{bmatrix} h_{x-el} & 0 \\ 0 & h_{el} \end{bmatrix} \begin{bmatrix} I(\dot{\theta})\cos(\phi) \\ I(\dot{\phi}) \end{bmatrix} \quad (50)$$

where  $I(\dot{\theta}) = 1$  if  $\dot{\theta} > 0$  and  $-1$  otherwise, similarly for  $\dot{\phi}$ . Model PFM5C estimates the coefficients to be  $-0''.54$  for azimuth and  $-0''.99$  for elevation.

Note that in the control system implementation this correction is multiplied by a hyperbolic tangent function of a scaled axis angular rate in order to prevent limit-cycle behavior of corrections when axis angular rates are small<sup>11</sup>.

#### 3.8.2 Alignment

The coupling between the axis backshaft and encoder can be modeled as a Hooke joint. Pointing error due to misalignment is then

$$\begin{bmatrix} \Delta\theta \\ \Delta\phi \end{bmatrix} = \begin{bmatrix} \frac{\cos(\gamma_a)\cos(\phi)}{1 - \sin(\gamma_a)^2 \sin(\theta)^2} \\ \frac{\cos(\gamma_e)}{1 - \sin(\gamma_e)^2 \sin(\theta)^2} \end{bmatrix} \quad (51)$$

where  $\gamma_a$  and  $\gamma_e$  are the azimuth and elevation encoder misalignments, respectively. For small misalignments this can be approximated by

$$\begin{bmatrix} \Delta\theta \\ \Delta\phi \end{bmatrix} = \begin{bmatrix} \lambda_{x-el} & 0 \\ 0 & \lambda_{el} \end{bmatrix} \begin{bmatrix} \cos(\phi)\cos(2\theta) \\ \cos(2\phi) \end{bmatrix}. \quad (52)$$

Note that the error is periodic in twice the axis angle which is distinct, with the exception of the tipping structure imbalance terms, from all other terms in the model. The current pointing model does not attempt to estimate or correct for this error. Design studies<sup>10</sup> predicted the error to be 1".41.

### 3.8.3 Cyclic error

Due to the design of the encoders, there is a fine-cycle error (periodic error over small angular excursions). Calibration data from one of the installed encoders<sup>12</sup> indicates a fine cycle error of approximately 1". The pointing model does not attempt to correct this error, nor is it clear that it is feasible to do so. The error can be considered as a zero-mean random contribution.

### 3.8.4 Nonlinearity

The same calibration indicates a maximum absolute difference (less cyclic error) of approximately 2".2. It may be possible to introduce encoder calibration tables into a pointing model to correct for this error, but the current model does not do so.

## 4 Additional modeling topics

### 4.1 Refraction correction

The difference between the ideal (encoder) and measured (astronomical) beam direction in ( 17 ) is determined at the aperture and hence atmospheric refraction effects must be removed<sup>11</sup>. The refraction model<sup>13</sup> has unknown error properties and these could be significant at very low elevations. This potential problem is circumvented by not using very low elevation data in model fits.

### 4.2 Inverting the model

The pointing model predicts error given a commanded azimuth and elevation: The GBT control system requires the opposite of this, i.e., the commanded azimuth and elevation that yield the desired pointing direction. The pointing model is implemented in the GBT control system as formulated here, and then an iterative (fixed-point) algorithm is used to determine the commanded angles that yield the desired pointing<sup>11</sup>.

### 4.3 Model parameter stability

Model parameters have physical interpretation, e.g., gravitational deflection of the feed arm, and it desirable that the inferences be stable from model fit to model fit. For example, if the gravitational terms show a drift over a long period or discontinuous change it would be an indication that the structure mass to stiffness ratio is changing, and could indicate impending problems with structural stability.

The current pointing model, PFM 5C, is a weighted least squares fit of 32 parameters (including thermal model terms) and used about 9900 astronomical measurements in the fitting process. The 2-norm condition numbers for azimuth model, elevation model, and focus model were respectively 75, 226, and 285. The large condition numbers indicate substantial sensitivity of the model to perturbations in the data such as noise in measurements and random effects from dataset to dataset, e.g. seasonal variations in the tilt of the azimuth track. Consequently model terms are not stable, and potentially are overfit even though the pointing measurement datasets are comparatively large.

Several alternatives to weighted least squares fitting, e.g. Tikhonov regularization and/or random effects modeling, could be used to improve the properties of the model fit. This will be discussed in the companion methods document.

#### 4.4 Error budgets

Some work has been done to characterize errors associated with data used for model fitting<sup>14</sup> in an effort to establish bounds on expected performance as well as mechanization of the performance specification<sup>1</sup>. Of particular note is the uncertainty in angular position of the astronomical sources that are used for pointing data collection<sup>15</sup>.

### 5 Parameter estimation topics

Given a model which is a subset of the model terms discussed above, the next problem is estimation of the model parameters. How does one go about estimating them, and what additional information, beyond the parameters themselves, is desirable? How does one go about collecting the data to fit to? How should these data be preprocessed before used for estimation? Detailed answers to these questions will be included in a companion document. Here's an overview.

The simplest approach to parameter estimation is to optimize the model with respect to a least-squares criterion. This method has nice properties in that the model is linear and the fit can be accomplished via the pseudo-inverse of the regressor matrix. If the errors in measurements are Gaussian, then the model fit is simultaneously the maximum-likelihood estimate of parameters and the Bayes optimal estimate. Supposing that we can estimate the parameters of an assumed Gaussian measurement error model (e.g., via a bootstrap), then one can use a weighted least squares estimate that has better outlier rejection properties. If the errors cannot be estimated, a reweighted least squares fit can be used to reject outliers.

Parameter estimates should have confidence intervals associated with them, both for determining the robustness of any one parameter value and so that some parameters can be used for diagnostics. For example, if a sequence of model fits over time indicate a 95% confidence that the stiffness of the feed arm has changed, the structure should be examined for incipient instability.

The condition number of the regressor matrices are large, indicating that some model terms are nearly linearly dependent. Thus small perturbations in measured data can result in large changes in the values of parameter estimates. This is undesirable for several reasons: Unstable parameter estimates disallow determining e.g. problems with structural stability, the physical meaning of the parameters is questionable, and the model will not generalize well, i.e., the data are over-fit. A very useful approach that mitigates the high condition number is to use some form of regularization to condition the estimates with prior knowledge. For example, model thermal coefficients can be bounded. While the resulting model fit will have e.g. higher squared error, it will perform better in practice.

Some model terms, e.g., the track model, almost certainly change substantially over time. When the data used to fit the model are taken over an extended interval in time (as they have been), these changes can result in poor fitting of other parameters. One approach to this problem is to employ random effects modeling which attempts to capture the variation in the parameter over subsets of the complete dataset.

There is a tendency to think that more data are better, but this is not always the case. In the previous paragraph we suggest that more data could cause deterioration of parameter accuracy unless special methods are used. It is also the case that there is a cost (lost observing time) associated with pointing data collection. Under a set of reasonable assumptions (error models) and given an objective for parameter accuracy and model performance, one can infer the amount of data that will be required.

### 6 Summary and recommendations

While the angular position of the main beam of the GBT is close-loop controlled using encoders on the mount axes, the actual position of the beam in topocentric coordinates is subject to a variety of perturbing

influences, both quasi-random and deterministic. This document is a consolidation of a variety of topics associated with the construction of a static pointing model for the GBT that includes geometrical, gravitational, thermal, track, wind, inertial, and non-ideal material effects.

Most of the recommendations that can be made are more closely associated with the estimation of parameters (see the section on parameter estimation topics). At this point in time the static (blind) pointing model appears to be good enough for GBT operations at 90 GHz. Some improvement could be made if it is possible to calibrate out encoder non-linearity. Dynamical errors during tracking due to GBT vibration, excited by the servo-control system or wind, are subject of some ongoing studies. It is also possible that more accurate thermal corrections could be had via a more dense sampling of structural temperatures and/or a better thermal model of the GBT including radiative and conductive transport.

---

<sup>1</sup> Condon, J. J., “Refined Scientific Requirements for the PTCS”, PTCS Project Note 27.2, December 2003.

<sup>2</sup> Srikanth, S., “GBT Pointing Coefficients”, GBT Memo 53, May 1990.

<sup>3</sup> TPOINT Software, <http://www.tpssoft.demon.co.uk/index.htm>.

<sup>4</sup> Condon, J. J., “GBT Pointing Equations”, GBT Memo 75.

<sup>5</sup> Constantikes, K. T., “Elevation Axle Pose Versus Elevation”, PTCS Project Note 46.0, March 2005.

<sup>6</sup> Lacasse, R., “The Green Bank Telescope Active Surface System”, GBT Memo 184.

<sup>7</sup> [http://www.engineeringtoolbox.com/young-modulus-d\\_773.html](http://www.engineeringtoolbox.com/young-modulus-d_773.html)

<sup>8</sup> Constantikes, K. T., “Thermally-Neutral Tradition Pointing Models and Thermal Corrections to Pointing and Focus”, PTCS Project Note 25.3, December 2003.

<sup>9</sup> Balsler, D. and Prestage, R., “Analysis of July 2003 Half-power Tracking Experiments”, PTCS PN19 (20 August 2003).

<sup>10</sup> “Pointing Accuracy”, GBT Technical Memorandum 52 Rev. 4, RSI (7 January 2000).

<sup>11</sup> Brandt, J., [http://wiki.gb.nrao.edu/pub/Software/ModificationRequest1C407/PTCS\\_Model5](http://wiki.gb.nrao.edu/pub/Software/ModificationRequest1C407/PTCS_Model5).

<sup>12</sup> “Acceptance Test Report for Serial Output Absolute Position Optical Encoder Model L696SSe-1, SN 920404”, BEI Motion Systems (17 January 2002).

<sup>13</sup> Condon, J., “Refraction Corrections for the GBT”, PTCS PN 35 (13 February 2004).

<sup>14</sup> Constantikes, K. T., “The GBT Pointing Model”, URSI 2007, Ottawa, Canada (26 July 2007).

<sup>15</sup> Condon, J., “The 2005 GBT Pointing Catalogue”, PTCS PN 39 (9 September 2005).

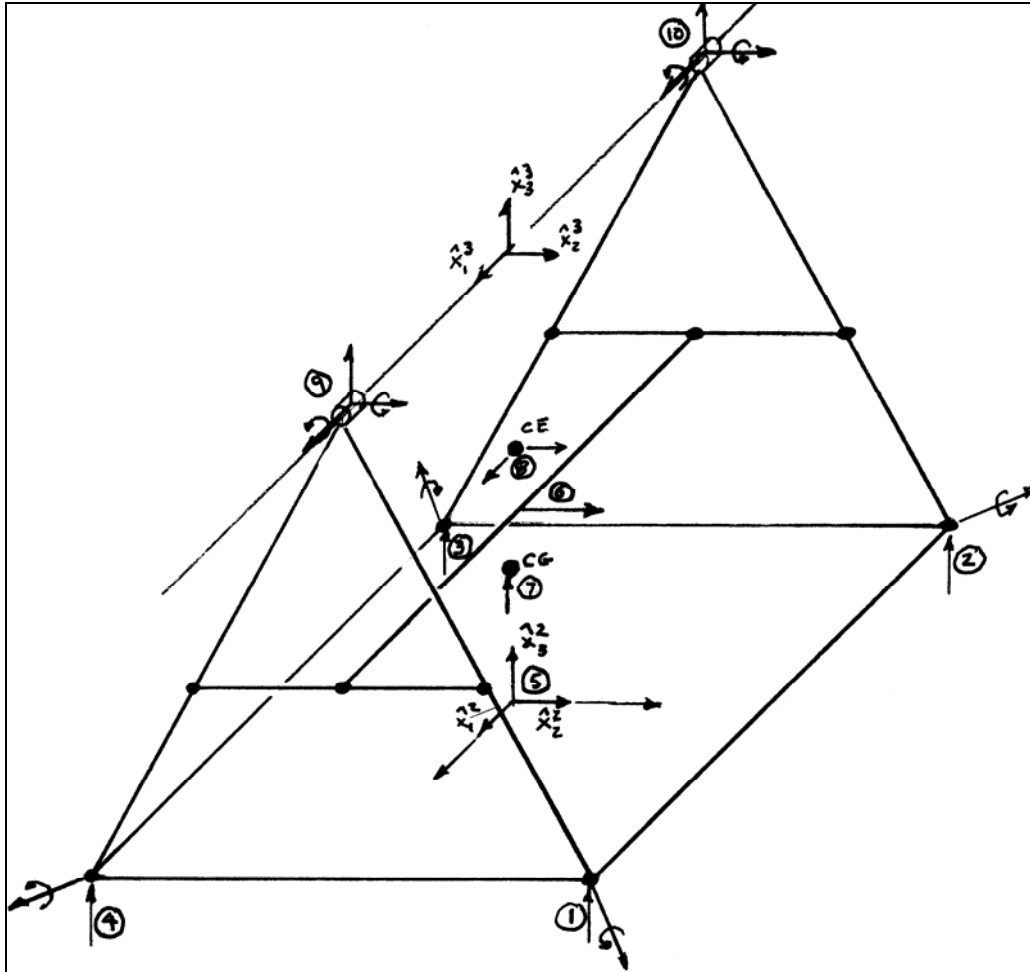


Figure 3. Alidade free body diagram.

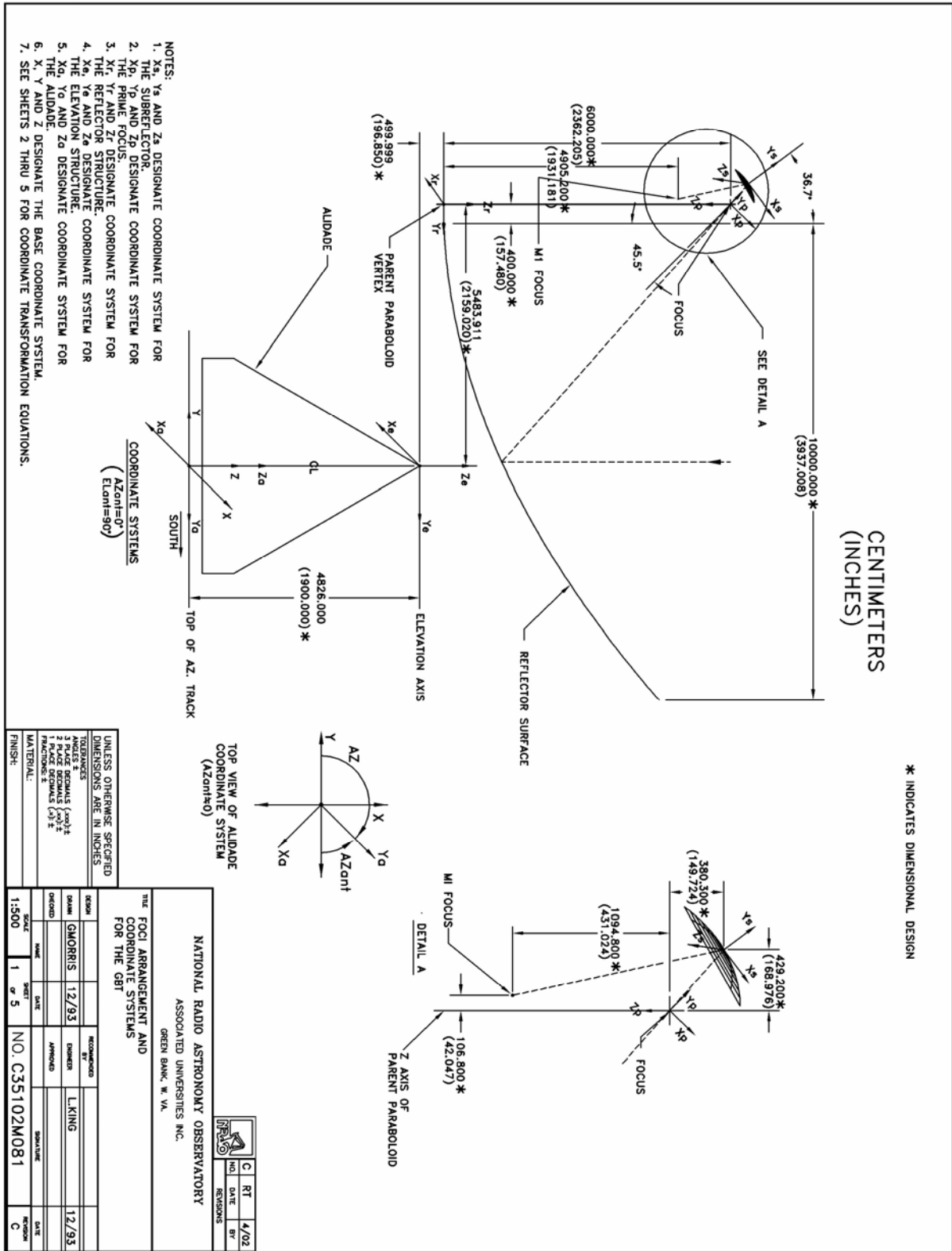


Figure 4. Foci Arrangements and Coordinate Systems for the GBT, Sheet 1.

**Definition of Coordinate Systems:**

1. The Base Coordinate System, (X, Y, Z).  
The base coordinate system is fixed to the ground. Its origin is at the intersection of the antenna azimuth axis and the top of the azimuth track. The positive directions of the axes are defined as follows:  
X-axis towards East  
Y-axis towards North  
Z-axis points up
2. The Alidade Coordinate System, (Xa, Ya, Za).  
The alidade coordinate system is attached to the alidade structure. It rotates about the antenna azimuth axis. Its position is defined by the azimuth antenna angle. The positive azimuth antenna angle (AZant) is measured from the negative Y axis in the counter-clockwise direction. When AZant is zero, the orientations of the axes are:  
Xa-axis towards West  
Ya-axis towards South  
Za-axis points up

The azimuth angle (AZ) is measured from the Y-axis and is positive in the clockwise direction looking from the positive Z side.

Therefore,  $AZ = 180 \text{ degrees} - AZ_{ant}$ . The transformation between the two coordinate systems, (1) and (2), are:

where

$$R_{12} = \begin{bmatrix} -1 & 0 & 0 \\ 0 & -1 & 0 \\ 0 & 0 & 1 \end{bmatrix} \begin{bmatrix} \cos(AZ_{ant}) & -\sin(AZ_{ant}) & 0 \\ \sin(AZ_{ant}) & \cos(AZ_{ant}) & 0 \\ 0 & 0 & 1 \end{bmatrix}$$

$$\begin{bmatrix} X \\ Y \\ Z \end{bmatrix} = R_{12} \begin{bmatrix} X_a \\ Y_a \\ Z_a \end{bmatrix}$$

UNLESS OTHERWISE SPECIFIED  
DIMENSIONS ARE IN INCHES

1 PLACE DECIMALS (0.00) ±	2 PLACE DECIMALS (0.00) ±	3 PLACE DECIMALS (0.000) ±
FRACTIONS: 1/8	FRACTIONS: 1/16	FRACTIONS: 1/32
FINISH:		



**C RT** 4/02  
NO. DATE BY  
REVISIONS

**NATIONAL RADIO ASTRONOMY OBSERVATORY**  
ASSOCIATED UNIVERSITIES INC.  
GREEN BANK, W. VA.

**TITLE**  
FOCI ARRANGEMENT AND  
COORDINATE SYSTEMS  
FOR THE GBT

DESIGN	DATE	APPROVED BY	DATE
GMORRIS 1/94	1/94	L KING	1/94
CHECKED	DATE	APPROVED	DATE
NAME	DATE	SIGNATURE	DATE
SHEET 2 of 5	NO. C35102M081		DATE
			REVISION C

Figure 5. Foci Arrangements and Coordinate Systems for the GBT, Sheet 2.

3. The Elevation Coordinate System, (Xe, Ye, Ze).

The elevation coordinate system is attached to the elevation structure. It rotates with the elevation structure defined by the elevation and the azimuth antenna angles. When the elevation antenna is 90°, Elant = 90°, its axes are positioned in the same directions as that of the alidade coordinate system. The relation between the Elevation and Alidade coordinate systems is given as follows:

$$\begin{bmatrix} X_a \\ Y_a \\ Z_a \end{bmatrix} = R_{23} \begin{bmatrix} X_e \\ Y_e \\ Z_e \end{bmatrix} + T_{23}$$

where

$$R_{23} = \begin{bmatrix} 1 & & & \\ & 0 & & \\ & \sin(\text{Elant}) & & \cos(\text{Elant}) \\ & -\cos(\text{Elant}) & & \sin(\text{Elant}) \end{bmatrix}$$

$$T_{23} = \begin{bmatrix} 0 \\ 0 \\ +1900.000 \end{bmatrix}$$

1900.00 is the height in inches of the elevation axis about the top of the track.

		CRT NO. DATE BY REVISIONS	4/02 1/94 C
NATIONAL RADIO ASTRONOMY OBSERVATORY ASSOCIATED UNIVERSITIES INC. GREEN BANK, W. VA.			
THE FOCI ARRANGEMENT AND COORDINATE SYSTEMS FOR THE GBT			
UNLESS OTHERWISE SPECIFIED DIMENSIONS ARE IN INCHES	DESIGN DRAWN CHECKED	RECOMMENDED BY DESIGNED APPROVED	DATE DATE DATE
TOLERANCES FRACTIONS: 1/16 DECIMALS: .001 HOLE DECIMALS: .001 HOLE FRACTIONS: 1/16 MATERIAL:	NAME DATE	SIGNATURE	DATE
FINISH:	SHEET 3 OF 5	NO. C35102M081	REVISION

Figure 6. Foci Arrangements and Coordinate Systems for the GBT, Sheet 3.

4. The Reflector Coordinate System, (Xr, Yr, Zr).  
 The reflector coordinate system is obtained by translations of the elevation coordinate system. This is shown in the following equation:

$$\begin{bmatrix} X_e \\ Y_e \\ Z_e \end{bmatrix} = \begin{bmatrix} X_r \\ Y_r \\ Z_r \end{bmatrix} + T_{34}$$

where

$$T_{34} = \begin{bmatrix} 0 \\ -2159.020 \\ 196.850 \end{bmatrix}$$

The offsets of the reflector paraboloid vertex from the elevation axis is given in inches by T34.

5. The Prime Focus Coordinate System, (Xp, Yp, Zp).

The origin of this coordinate system is at the focus of the dish paraboloid, 2362.205 inches from vertex of the paraboloid on the Zr-axis. Yp-axis is 45.5° from Zr-axis on the ZrYr plane, and the Zp-axis is parallel to the Xr-axis. The transformation is as follows:

$$\begin{bmatrix} X_r \\ Y_r \\ Z_r \end{bmatrix} = R_{45} \begin{bmatrix} X_p \\ Y_p \\ Z_p \end{bmatrix} + T_{45}$$

where

$$R_{45} = \begin{bmatrix} 0 & 0 & 1 \\ \cos(45.5^\circ) & -\sin(45.5^\circ) & 0 \\ \sin(45.5^\circ) & \cos(45.5^\circ) & 0 \end{bmatrix}$$

$$T_{45} = \begin{bmatrix} 0 \\ 0 \\ 2362.205 \end{bmatrix}$$

		C RT 4/02 NO. DATE BY REVISIONS
NATIONAL RADIO ASTRONOMY OBSERVATORY ASSOCIATED UNIVERSITIES, INC. GREEN BANK, W. VA.		
TITLE FOCI ARRANGEMENT AND COORDINATE SYSTEMS FOR THE GBT		
UNLESS OTHERWISE SPECIFIED DIMENSIONS ARE IN INCHES	DESIGNED BY L. KING	DATE 1/94
TOLERANCES 1 FRACTIONS 2 PLACE DECIMALS (.00)± 3 PLACE DECIMALS (.001)± 4 PLACE DECIMALS (.0001)± FRACTIONS 1/16 1/32	CHECKED BY APPROVED BY	SCALE 4" = 5'
MATERIAL:	NO. C35102M081	REVISION C

Figure 7. Foci Arrangements and Coordinate Systems for the GBT, Sheet 4.

6. The Subreflector Coordinate System, (Xs, Ys, Zs).  
 The axes of this coordinate system are orientated similarly as that of the prime focus coordinate system. The angle between Ys-axis and Zr-axis is 36.7°. By the same token, we have:

$$\begin{bmatrix} X_r \\ Y_r \\ Z_r \end{bmatrix} = R_{46} \begin{bmatrix} X_s \\ Y_s \\ Z_s \end{bmatrix} + T_{46}$$

where

$$R_{46} = \begin{bmatrix} 0 & 0 & 1 \\ \cos(36.7^\circ) & -\sin(36.7^\circ) & 0 \\ \sin(36.7^\circ) & \cos(36.7^\circ) & 0 \end{bmatrix}$$

$$T_{46} = \begin{bmatrix} 0 \\ -168.976 \\ 2511.929 \end{bmatrix}$$

7. Examples:

a. For a point L from the reflector coordinates to the base coordinates.

$$\begin{bmatrix} X \\ Y \\ Z \end{bmatrix}_L = R_{12} \begin{bmatrix} X_r \\ Y_r \\ Z_r \end{bmatrix} + T_{23}$$

b. For a point M from the base coordinates to the reflector coordinates.

$$\begin{bmatrix} X_r \\ Y_r \\ Z_r \end{bmatrix}_M = R_{23}^{-1} \begin{bmatrix} X \\ Y \\ Z \end{bmatrix}_M - T_{23}$$

		C RT 4/02 NO. DATE BY REVISIONS
NATIONAL RADIO ASTRONOMY OBSERVATORY ASSOCIATED UNIVERSITIES INC. GREEN BANK, W. VA.		
TITLE <b>FOCI ARRANGEMENT AND                  COORDINATE SYSTEMS                  FOR THE GBT</b>		
UNLESS OTHERWISE SPECIFIED DIMENSIONS ARE IN INCHES		
TOLERANCES 1 PLACE DECIMALS (0.00) ± 2 PLACE DECIMALS (0.00) ± 3 PLACE DECIMALS (0.00) ± FINISHES: 1 MATERIAL:		
DESIGN DRAWN CHECKED NAME DATE	RECOMMENDED BY CHECKED APPROVED SIGNATURE DATE	NO. C35102M081 SHEET 5 OF 5

Figure 8. Foci Arrangements and Coordinate Systems for the GBT, Sheet 5.

